SiON Integrated Optics Elliptic Couplers for Fizeau-Based Optical Coherence Tomography

Van Duc Nguyen, Nur Ismail, Fei Sun, Kerstin Wörhoff, Ton G. van Leeuwen, and Jeroen Kalkman

***Abstract*—Integrated optics potentially can offer significant cost reductions and new applications to Optical Coherence Tomography (OCT). We design, fabricate, and characterize Silicon oxynitride (SiON) elliptic couplers, which can be used to focus light from a chip into the off-chip environment. Fizeau-based OCT measurements are performed with elliptic couplers and a moveable mirror. The optical fields at the output of the elliptic coupler are simulated and measured. Good agreement is observed between the measured OCT signal as a function of depth and calculations based on the optical field at the end of the elliptic coupler.**

***Index Terms*—Elliptic couplers, integrated optics, optical coherence tomography.**

I. Introduction

OPTICAL coherence tomography (OCT) [1] is a non-invasive optical technique for imaging biological tissue to a few millimeters depth with micrometer resolution. OCT is gaining widespread use in the clinic, in particular its use in ophthalmology for imaging the retina is becoming routine practice. OCT is analogous to ultra-sound as it measures the time-of-flight of photons. However, OCT uses low coherence interferometry instead of electronic timing to detect the time-of-flight. Currently, most OCT systems are Fourier-domain OCT systems, measuring the interference spectrum, formed by the reflection from the tissue and the reference arm, either by using a spectrometer or a swept source. These OCT systems consist of a large number of bulk optical components, such as: optical fibers, (focusing) lenses, beam splitters, and galvanometric scanners. All these components are necessary to relay the optical signal through the OCT system, thereby making OCT systems bulky, expensive, and complex. Integrated optics can make OCT systems smaller and more cost efficient. In addition, integrated optics can add functionality that would be too difficult, or complex, to achieve with bulk optics.

Although some work on miniaturizing OCT components and devices has been performed [2], [3], most work mainly focuses on achieving a size reduction using smaller bulk optical components and/or designing them in a more compact way. However, the use of integrated optics can offer much higher integration density, which can lead to systems with a significantly smaller footprint. Many of the integrated-optics components, similar to those that can be used for OCT, already have been designed and fabricated for optical telecommunication. However, it remains a challenge to modify their design in such a way that they are suited for OCT. Currently, integrated optics only has been used in a time-domain OCT system, replacing the optical fibers and splitters, with all other components external to the optical chip [4]. Here we show the design and fabrication in integrated optics of another component used with OCT: an optical focuser.

Similar to confocal microscopy, in OCT light is focused onto the sample through a lens and the back scattered light is collected through the same lens. Focusing of the beam gives OCT lateral resolution (determined by the spot size) and reduces the collection of multiple scattered light (confocal gating). Since OCT uses broadband illumination of the sample, the focusing optics is generally done by achromatic lenses.

Focusing light can be performed by diffraction, refraction, and/or reflection. In integrated optics various diffracting structures, such as waveguide grating couplers [5] and Fresnel-grating lenses [6], have been designed to focus light a few millimeters into the off-chip environment. These techniques have two drawbacks. First, they require electron beam lithography to define the diffractive structures. Electron-beam lithography is costly, complicated, and not suitable for high-throughput applications. Second, diffractive techniques are, by nature, chromatic, therefore tight focusing with broadband light sources, as are used in OCT, is difficult. Integrated optics structures based on refraction, such as aspheric waveguide lenses, were designed and fabricated using standard photolithography techniques [7], [8]. Refractive surfaces of waveguide lenses show chromatic aberrations and have internal reflection losses. Both are a disadvantage for application to OCT. Integrated optics structures using reflection, such as planar mirrors [9] and elliptic couplers [10], do not suffer from high losses and are achromatic. Planar mirrors were designed for collimation, but also can be used for focusing. However, planar mirrors need a large footprint and typically they focus under an angle relative to the input waveguide. Low-loss and compact elliptical couplers were created for focusing/collimating beams in the off-chip region. We will discuss integrated-optics elliptic couplers in more detail.

II. Elliptic Coupler Structure

An elliptic coupler consists of a straight index guiding planar strip waveguide followed by one half of a planar elliptic-shaped

Manuscript received February 23, 2010; revised June 24, 2010; accepted July 23, 2010. Date of publication August 12, 2010; date of current version September 22, 2010. This work was supported by the Smart Mix Program of the Netherlands Ministry of Economic Affairs and the Netherlands Ministry of Education, Culture and Science.

V. Duc Nguyen, T. G. van Leeuwen, and J. Kalkman are with the Biomedical Engineering and Physics Department, Academic Medical Center, University of Amsterdam, NL 1100 DE Amsterdam, The Netherlands (e-mail: d.v.nguyen@amc.nl, t.g.vanleeuwen@amc.nl, j.kalkman@amc.nl).

N. Ismail, F. Sun, and K. Wörhoff are with the Integrated Optical MicroSystems Group, MESA + Institute for Nanotechnology, University of Twente, Enchede, The Netherlands (e-mail: n.ismail@ewi.utwente.nl, f.sun@ewi.utwente.nl, k.worhoff@ewi.utwente.nl).

Digital Object Identifier 10.1109/JLT.2010.2066958

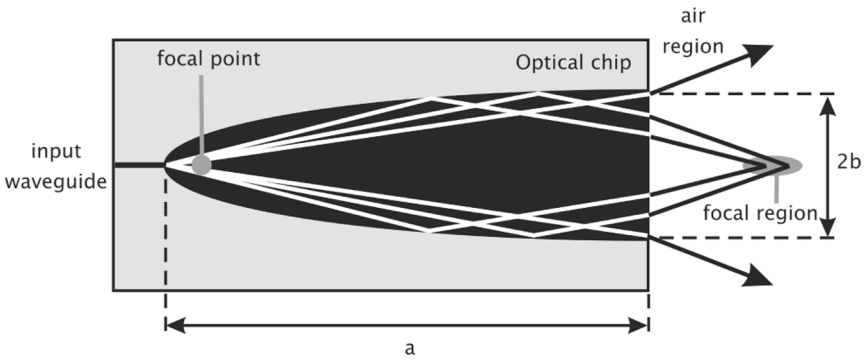

Fig. 1. In-plane schematic of an elliptic coupler with dimensions (a, b) for the two semi-axis.

index guiding section, as is shown in Fig. 1. The dimensions of the elliptic coupler are determined by the semimajor axis a and semiminor axis b. We will denote an elliptic coupler by the combination (a, b) with a and b in micrometers. The focusing principle of elliptic couplers can be described in two ways.

In a ray optics description, all rays emanating from one focal point of a full ellipse are imaged onto the second focal point. Since, the straight waveguide exits close to the first focal point, it is thus to be expected that many rays will be imaged close to the second focal point. In case of a half elliptic coupler ending in an air region, the rays refract away from the normal at the interface thereby reducing the focal length in the air region. In addition, some rays originating from the waveguide with low exit angles are not reflected from the ellipse boundary and travel unfocused into the air region, these are the divergent rays.

In a Gaussian optics field description, the field at the exit of the elliptic coupler is a spherical wave with a radius of curvature equal to the length a divided by the effective index of the waveguide [10]. The unfocused beam acts as a diverging optical field superimposed on the converging optical field. Gaussian field calculations are accurate only when the diverging field has a relatively small magnitude. The full field at the exit of the waveguide/elliptic coupler can be determined using Beam Propagation Method (BPM) simulations.

In this paper we design and fabricate elliptic couplers in SiON technology [11]. SiON is an amorphous material with excellent electrical, optical and mechanical properties. The refractive index of SiON for wavelengths in the infrared of SiON can be adjusted from 1.46 (silicon dioxide) to 2.0 (silicon nitride). Particularly attractive for optical applications is the high transparency of silicon oxynitride over a large wavelength range, from visible to infrared, covering all of the commonly used OCT wavelengths of 800, 1000, and 1300 nm.

We characterize the focusing properties of the elliptic couplers by optical beam-profiling measurements and BPM simulations. The elliptic couplers are used in a Fizeau-based spectral-domain OCT system [12]. We analyze the OCT signal magnitude variation with depth caused by the focusing properties of these couplers and compare this to calculations based on the optical beam profile measurements. Finally we make recommendations on further improvements in the focusing properties of integrated optics couplers for OCT and other applications.

III. Material and Methods

A. Waveguide and Elliptic Coupler Design and Fabrication

Waveguides are designed and fabricated in SiON technology. This technology uses $\langle 100 \rangle$-oriented 100-mm Si wafers that are first thermally oxidized to obtain an 8 μm thick SiO_2 layer. Next an 820 nm thick SiON layer is grown using plasma enhanced chemical vapor deposition. This is followed by thermal annealing to achieve the desired thickness and refractive index of $\mathrm{n} = 1.5175$ for quasi-TE polarization at 1300 nm wavelength. The SiON layer is etched through by reactive ion etching to achieve channel waveguides. The straight waveguides and elliptic coupler structures are covered with a SiO_2 layer deposited with plasma enhanced chemical vapor deposition. After annealing the refractive index of the upper-cladding oxide is 1.4485 for quasi-TE polarization at 1300 nm wavelength, the same to that of the bottom-cladding thermal oxide layer.

We performed mode field calculations (FieldDesigner, PhoeniX bv., Enschede, The Netherlands) using the dimensions and refractive indexes stated above. The waveguides show single mode operation for waveguide widths smaller than 3 μm at 1300 nm wavelength. We choose a waveguide width of 2.5 μm for our waveguide design. We make use of the effective index method [13] to find an equivalent 2-D structure to represent our 3-D waveguide geometry. This leads to the choice of core and cladding indexes of $n_{\mathrm{core}} = 1.476$ and $n_{\mathrm{clad}} = 1.447$, respectively. Two-dimensional BPM simulations [13] (OptoDesigner, PhoeniX bv., Enschede, The Netherlands) are used to simulate the electric field (quasi-TE polarization) from a straight waveguide and various elliptic couplers both within the elliptic couplers and in the air region.

B. Experiments

A schematic of our experimental setup is shown in Fig. 2. Light from a broadband source (AFL technologies, center wavelength $\lambda_{\mathrm{c}} = 1275$ nm, 45 nm bandwidth, 25 mW output power) is coupled into an optical circulator (Gould Fiber Optics). The output port of the optical circulator is connected to a tapered fiber (OZ Optics, TSMJ-3S-1550-9). The tapered fiber is coupled to the waveguide using a high precision XYZ stage (Elliot Scientific). We measured 10 dB fiber-to-chip coupling loss (single pass).

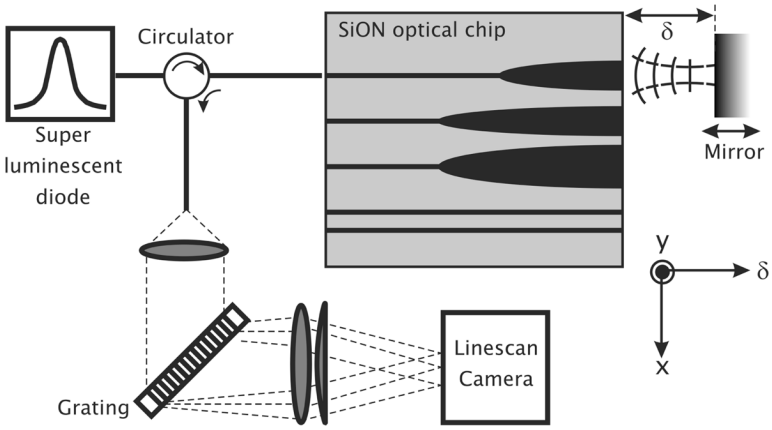

Fig. 2. Schematic of the experimental setup used for Fizeau-based OCT measurements on an optical chip. For optical beam profiling measurements a knife edge is placed at a distance δ from the output facet.

For optical beam profiling of the horizontal waists (in the plane of the chip) we use a razor blade mounted on a motorized linear stage (Zaber T-LS13-M). Light transmitted through the waveguide is collected at the output facet of a chip with a high NA lens. A knife is translated slowly through the beam between the end-facet of the chip and the lens, the light intensity is measured as a function of position with an optical power meter (Newport, model 840-C). The thus measured integrated intensity profile is differentiated and fitted with a Gaussian function to determine the $1/\mathrm{e}^2$ intensity beam waist [14]. For the smaller vertical waist (out of the plane of the chip), we use the intensity transmitted into a well-characterized high numerical aperture collection fiber positioned at a few positions in the vertical plane. From the collected intensity the vertical waveguide numerical aperture was determined.

For Fizeau-based OCT measurements, light from the waveguide/elliptic coupler is reflected on a mirror which is at a depth δ opposite to the waveguide/elliptic coupler end facet. The light reflected from the mirror is coupled back into the waveguide/elliptic coupler, the light reflected from the end facet (Fresnel reflection) serves as the reference field. Both fields are re-directed by the optical circulator to the spectrometer. The spectrometer consists of an achromatic collimator lens that directs the beam on a volume transmission grating (Wasatch Photonics, 1145 lines/mm). The collimated beam is imaged with a lens doublet onto a 46 kHz CCD linescan camera (Sensors Unlimited SU-LDH-1.7RT/LC. More details can be found in [15]. The system sensitivity roll-off is measured and corresponds to a ratio of optical resolution over pixel resolution $\omega = 1.1$ [16]. The measured spectra are processed in the following order: 1) reference arm subtraction 2) dispersion compensation 3) spectral re-sampling to linear k-space. The thus obtained optical spectrum is Fourier transformed to a depth scan, with the magnitude of the complex signal taken as the OCT signal. To compare the OCT signals in depth to theoretical calculations, the depth scans are corrected for the spectral-domain system sensitivity [16].

C. Optical Field and OCT Signal Response Calculations

We calculate the electromagnetic fields and the OCT signal response in the air region. We assume that the field at the output facet of the waveguide/elliptic coupler is a simple two-dimensional Gaussian distribution (neglecting the divergent field part). Therefore, the total field in the air region can be written as the product of a horizontal, designated by x (in the plane of the optical chip) and a vertical part, designated by y (perpendicular to the plane of the chip). The horizontal part is a Gaussian field focused at a depth $f \neq 0$, and the vertical part is a non focused Gaussian field, $f = 0$. The total field amplitude (neglecting the phase part) is

$$\Psi(x,y,\delta) = \sqrt{\frac{2}{\pi w_x(\delta) w_y(\delta)}} e^{-\frac{x^2}{w_x^2(\delta)}} e^{-\frac{y^2}{w_y^2(\delta)}} \tag{1}$$

with δ the coordinate in the propagation direction relative to the waveguide/elliptic coupler end facet, $w_x(\delta)$ and $w_y(\delta)$ are the waists in the horizontal and vertical plane, respectively.

The waist development for the two directions is given by the standard description for a Gaussian field, $f \neq 0$ for the horizontal (focusing) plane

$$w_x(\delta) = w_{0x}\sqrt{1 + \left(\frac{\delta - f}{Z_x}\right)^2} \tag{2}$$

and with $f = 0$ for the vertical plane

$$w_y(\delta) = w_{0y}\sqrt{1 + \left(\frac{\delta}{Z_y}\right)^2} \tag{3}$$

with $Z_{x,y}$ the Rayleigh ranges in the x and y direction, w_{0x} the beam waist (beam radius at the $1/\mathrm{e}^2$ intensity level) at the focal point and w_{0y} the beam waist at the output facet of the waveguide/elliptic coupler. Since $Z_{x,y} = \pi(w_{0x,y})^2/\lambda_c$, the whole field development in the air region can be calculated by using a measured field waist and focal length.

Since OCT measures the field in the probing range, the OCT signal response to a mirror can be calculated based on the square root of the intensity transmission function [17], [18]. If we assume a 100% reflective mirror, perpendicularly aligned to the

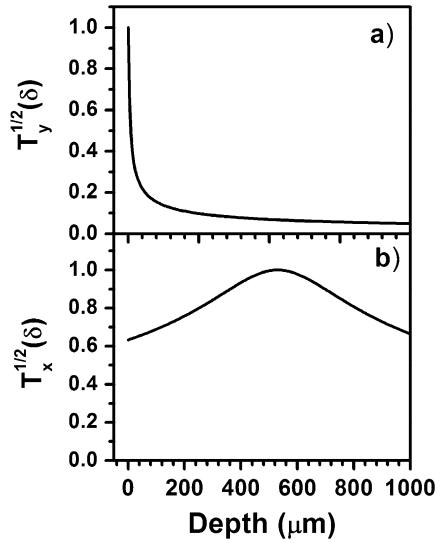

Fig. 3. OCT transmission functions as a function of depth for the vertical (a) and horizontal (b) direction for an elliptic coupler with $f = 530\ \mu$m, $w_{0x} = 9.8\ \mu$m, $w_{0y} = 1.0\ \mu$m.

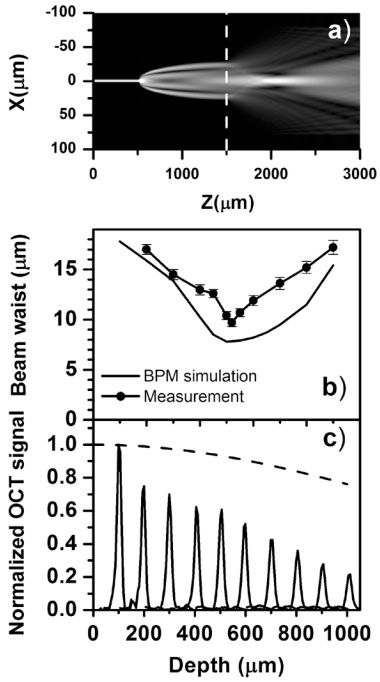

Fig. 4. (a) BPM optical field amplitude simulation for the elliptic coupler with $(a, b) = (1000, 35)$. The dashed line indicates the border between the chip and the air region. (b) Beam waists in the air region for the BPM simulation (solid line) and the knife edge measurements (dots and line). (c) Measured OCT signal as a function of depth for a mirror reflector. The dashed line indicates the spectral-domain system sensitivity; the OCT signal shown here is not corrected for the spectral-domain sensitivity.

chip facet, located in the air region at depth δ from the waveguide/elliptic coupler, the OCT signal magnitude $|a_{\mathrm{OCT}}|$ as a function of depth δ is calculated using standard overlap integrals

$$|a_{\mathrm{OCT}}| = \sqrt{T(\delta)} = \sqrt{T_x(\delta)} \cdot \sqrt{T_y(\delta)} = \frac{1}{\left[\left(\frac{(\delta - f)}{Z_x}\right)^2 + 1\right]^{1/4}} \frac{1}{\left[\left(\frac{\delta}{Z_y}\right)^2 + 1\right]^{1/4}} \quad (4)$$

with $T_x(\delta)$ and $T_y(\delta)$ the intensity transmission functions in the horizontal and vertical planes, respectively. The square roots of the intensity transmission function we name the "OCT transmission function".

For illustrative purposes, Fig. 3 shows a plot of OCT transmission function $(\mathrm{T_x})^{1/2}$ and $(\mathrm{T_y})^{1/2}$ calculated with a set of parameters that are typical for an elliptic coupler ($f = 530\ \mu$m, $w_{0x} = 9.8\ \mu$m, $w_{0y} = 1.0\ \mu$m). The OCT transmission in the vertical direction drops rapidly with depth δ as the field is strongly diverging in the vertical plane, whereas the OCT transmission in the horizontal direction shows a maximum at the focal point.

IV. Results

We investigated the following structures: straight waveguide and elliptic couplers with $(a, b) = (1000, 35), (2000, 35)$, and $(2000, 65)$. For every structure we performed the following analysis: 1) BPM simulations 2) knife edge measurements of the optical field intensity in air 3) Fizeau OCT measurements with varying mirror depth δ.

Fig. 4 shows these steps for the elliptic coupler with $(a, b) = (1000, 35)$. Fig. 4(a) shows the BPM simulation of the electric field amplitude (quasi-TE polarization) in the horizontal plane, both within the elliptic coupler and in the air region. The dashed line indicates the end-facet of the coupler. We can observe that the optical field is converging in the air region as expected.

Fig. 4(b) shows knife-edge method beam waist measurement at various depths δ (dots). The measurements are in good agreement with the BPM simulation (solid line). The overestimation of the measured beam waist is attributed to the fact that the field is not purely Gaussian and that there is a contribution from the divergent field (see Fig. 4(a)). Knife-edge measurements and BPM simulations for the optical fields in the plane of the chip are performed for a straight waveguide and various elliptic couplers, as summarized in Table I. For all structures studied good agreement between the measurements and the simulations is observed.

Fig. 4(c) shows the normalized OCT signal for varying depth δ. At 100 μm depth, the OCT resolution is 17 μm and the signal to noise ratio is 55 dB, measured for a single spectrum at 46 kHz. The resolution remains constant over the depth range used in this experiment. The OCT signal drops in depth due to a decrease of the spectral-domain system sensitivity (as indicated by the dashed line) and due to the field development in the air region. Since the field diverges strongly in the vertical direction, the reflected electric field decreases with increasing depth δ.

A quantitative comparison of the OCT signal magnitude as a function of depth for the four structures summarized in Table I is shown in Fig. 5. The straight waveguide, Fig. 5(a), shows a rapid decrease of peak OCT signal with depth due to the strongly diverging fields both in the vertical and horizontal planes. Similar measurements are presented in Fig. 5(b), (c), and (d) for the three elliptic couplers with $(a, b) = (1000, 35), (2000, 35)$

TABLE I
ELLIPTIC COUPLER BEAM WAISTS AND FOCAL LENGTHS

a	*b*	*f* ***(BPM)***	*f* ***(Exp.)***	w_{0x} ***(BPM)***	w_{0x} ***(Exp.)***	w_{0y} ***(BPM)***	w_{0y} ***(Exp.)***
∞	**1.25**	0	-	1.1	1.3 ± 0.1	0.8	1.0± 0.2
1000	**35**	500	530	7.8	9.8 ± 0.5	0.8	1.0± 0.2
2000	**35**	650	750	12.2	16.0 ± 1.1	0.8	1.0± 0.2
2000	**65**	1300	1330	9.6	12.1 ± 0.7	0.8	1.0± 0.2

Beam waists and focal lengths for a straight waveguide and various elliptic couplers (all lengths are in microns). Beam waists and focal lengths are measured experimentally and simulated with BPM. The elliptic coupler dimensions are denoted with (a,b), where a is the semi-major axis length and b is the semiminor axis length, (a,b)=(∞,1.25) indicates a straight waveguide of 2.5μm width.

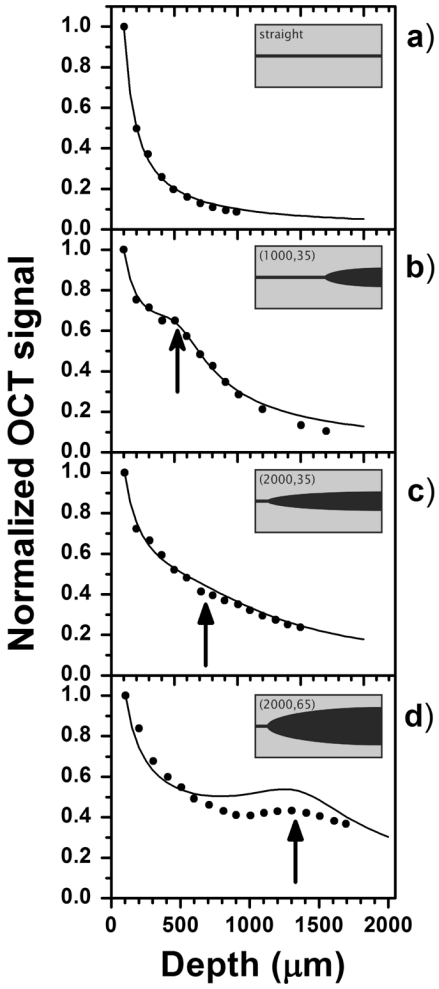

Fig. 5. OCT signal magnitude versus depth for a mirror reflector (dots). The measurements are compared calculations of the square root of the transmission function, which is based on the measured beam waists for: (a) single straight waveguide and (b),(c),(d) different elliptic couplers with dimensions $(a, b) = (1000, 35), (2000, 35), (2000, 65)$, respectively. The OCT signal magnitude is normalized to the value at 100 μm from the end-facet of the waveguide/elliptic coupler and corrected for spectral-domain sensitivity. Arrows indicate the measured focal point for every elliptic coupler.

and $(2000, 65)$, respectively. Clearly, the focusing enhances the OCT signal in the air region near the chip end facet.

The OCT measurements are compared to calculations (solid lines) based on (4) and the measured focal length, horizontal and vertical beam waist. The OCT signal from the straight waveguide is described by taking $f = 0$. The OCT signal is normalized to the measurement at 100 μm depth, which is the minimum depth at which we could measure. Note that at this depth the total field already has dropped significantly due to the strong vertical beam divergence (the first factor in (4)). However, since this factor is assumed constant for all structures (depending only on the vertical waveguide size) we can quantitatively compare the OCT signals for the different structures. For all structures good agreement between the calculations and the OCT measurement can be observed. The differences between the measurements and the calculations are attributed to the non-Gaussian field distribution at the end of the elliptic coupler. In our calculations this was not taken into account. We observe a 10–20 fold sensitivity increase of the OCT signal at the focal point for every elliptic coupler compared to the straight waveguide.

V. DISCUSSION

In this study we characterize the focusing properties of the elliptic couplers by BPM simulations, optical beam-profiling measurements and the OCT signal decrease with depth.

Good agreement is achieved between the OCT measurements and beam profile measurements for the four structures we have presented. In addition, the measured beam waists are in good agreement with the BPM simulations. For elliptic couplers with other (a, b) dimensions, which are not shown here, the results show somewhat poorer agreement due to the large strength of the unfocused beam for these structures. As a result, the optical fields in the air region are not purely Gaussian, as is also observed from the BPM simulations and from beam profile measurements for these structures. However, using a full optical field description, either from BPM simulations or full 3-D beam profiling measurements, the OCT signal in principle also can be calculated for these structures, albeit with more effort.

The 55 dB OCT sensitivity that we typically measure is lower than measured with an equivalent fiber based system [15] mainly due to the high in/out fiber-to-chip coupling losses (see Section III.B). With improved fiber-to-chip coupling (e.g., using index matching gel) we expect a sensitivity that can be 20 dB higher. However, the current sensitivity should be sufficient to image a limited spatial extend <1 mm (see also [2]). Using elliptic couplers with OCT changes in flow, refractive index, and morphology can be monitored in small (flow) channels, e.g., located on a combined optical/fluidic chip.

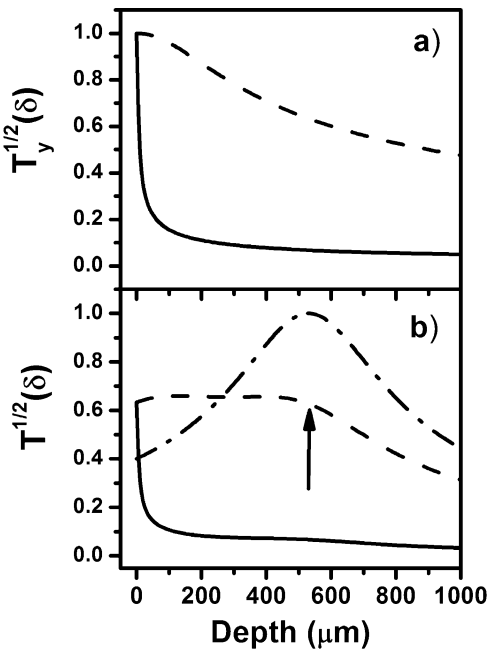

Fig. 6. Theoretical calculations for (a): OCT transmission function $(\mathrm{T_y})^{1/2}$ in the vertical plane with $w_{0y} = 1.0\,\mu$m (solid line) and 9.5 μm (dashed line) and (b): the OCT signal, $(T)^{1/2}$, response with a mirror reflector for elliptic coupler (1000,35) with $(w_{0x}, w_{0y}) = (9.8\mu\mathrm{m}, 1.0\mu\mathrm{m})$ (solid line) and $(9.8\mu$m, 9.5μm)(dashed line) compared with ideal lens ($f = 530\mu$m, $w_0 = 9.8\mu$m) (dash-dotted line). An arrow indicates the focal points.

The Fizeau-OCT signal decreases strongly in depth due to the large divergence of the beam in the vertical direction. Equation (4) shows that the OCT signal drop-off in depth can be improved by decreasing the divergence of the field in the vertical direction. In other words, the OCT performance can be enhanced if the beam waist is increased in the vertical plane (the field divergence angle in Gaussian optics is inversely proportional to the beam waist [19]). Increasing the beam waist in the vertical plane can be achieved by reducing the overall waveguide height. However, this would result in poorer light guiding due to a reduction of the effective index contrast. The resulting increase in bending losses and decreasing coupler focusing efficiency makes this method less favorable. Therefore, a relatively short tapered section at the end of the elliptic coupler region will result in high optical confinement in the waveguides and a large beam waist at the exit of the elliptic coupler.

Vertical tapering can be performed in various ways [20]. For SiON a vertical taper can be fabricated by depositing a sacrificial layer on top of the SiON waveguide. If the sacrificial layer has a higher etch rate than silicon oxynitride for the specific etchant used in the process (e.g., buffered HF) a waveguide taper is formed. We estimated that the minimum SiON waveguide thickness that can be achieved is 0.2 μm. For a waveguide thickness of 0.2 μm, field simulations show that the beam waist in the vertical plane can increase up to 9.5 μm, which decreases the field divergence by a factor 10. Based on this field development in the vertical direction we calculate the OCT transmission function and the OCT signal drop off in depth for an elliptic coupler (1000, 35), a similar elliptic coupler with taper, and an ideal lens. Fig. 6(a) shows the OCT transmission function in the vertical plane, $(\mathrm{T_y})^{1/2}$, with $w_{0y} = 1.0\,\mu$m and 9.5 μm (with taper), respectively.

Fig. 6(b) shows the OCT signal in depth, $\mathrm{T}^{1/2}$, for the elliptic coupler with and without taper and for an ideal lens ($f = 530\,\mu$m, beam waist at focus $w_0 = 9.8\,\mu$m). The OCT signal of the elliptic coupler is enhanced strongly in depth as a result of a decrease of the divergence of the field in the vertical plane (as shown in Fig. 6(a)). At the focal point, a 10 fold sensitivity increase of the OCT signal can be observed. Although, the OCT signal for the ideal lens shows a higher sensitivity around the focus, the tapered elliptic coupler has a high and constant sensitivity over a long range (600 μm) from the end facet of the tapered elliptic coupler to the focal point.

Note that an ideal integrated optics elliptical taper also has an elliptic shape in the vertical direction. However, such an ideal structure is very complicated to reproducibly fabricate using dry/wet etching techniques.

Fizeau interferometers have the advantage that they are so-called common-path interferometers. Consequently, they do not suffer from dispersion mismatch between sample and reference arm since the light travels back and forth through the same path. On the other hand, the imaging range is limited to a few millimeters from the final reflection (in our case the end facet of the waveguide/elliptic coupler). Therefore, in Fizeau-based OCT systems there is no space available at the exit of the elliptic coupler for a lateral sample scanner, or any other optical component.

Most common day OCT systems are Michelson interferometers in which the reference arm length can be set at an arbitrary length relative to the sample arm. Therefore, in Michelson interferometers an arbitrary amount of space can be made available at the end of the sample arm to host a lateral sample scanner or any other optical component. A next step is to implement elliptic couplers in a Michelson type interferometer with a loop mirror reference arm, which will lead to further OCT system integration on an optical chip.

Finally, the focusing properties of these elliptic couplers also can be used to improve the detection sensitivity performance in other integrated optics sensing applications.

VI. Conclusion

In this paper, we showed the feasibility of an integrated optics elliptic coupler for OCT fabricated in SiON. The OCT signals for various elliptic couplers were measured and showed good agreement with calculations based on measured beam waists. We made recommendations on improving the focusing properties of integrated optics couplers for OCT and other applications.

Acknowledgment

The authors would like to thank Gabriël Sengo for the fabrication of the channel waveguides and Rene de Ridder for helpful discussions.

References

[1] D. Huang *et al.*, "Optical coherence tomography," *Science*, vol. 267, pp. 1178–1181, 1991.

[2] K. M. Tan *et al.*, "In-fiber common-path optical coherence tomography using a conical-tip fiber," *Opt. Exp.*, vol. 17, pp. 2375–2384, 2009.
[3] B. D. Goldberg, S. M. R. M. Nezam, P. Jillella, B. E. Bouma, and G. J. Tearney, "Miniature swept source for point of care optical frequency domain imaging," *Opt. Exp.*, vol. 17, pp. 3619–3629, 2009.
[4] D. Culemann, A. Knuettel, and E. Voges, "Integrated optical sensor in glass for optical coherence tomography (OCT)," *IEEE J. Select. Topics Quantum Electron.*, vol. 6, no. 5, pp. 730–734, Sep./Oct. 2000.
[5] S. Ura, Y. Furukawa, T. Suhara, and H. Nishihara, "Linearly focusing grating coupler for integrated-optic parallel pickup," *J. Opt. Soc. Amer. A*, vol. 7, pp. 1759–1763, 1990.
[6] P. R. Ashley and W. S. C. Chang, "Fresnel lens in a thin-film waveguide," *Appl. Phys. Lett.*, vol. 33, pp. 490–492, 1993.
[7] D. Y. Zang, "Waveguide optical planar lenses in $LiNbO_3$—Theory and experiments," *Opt. Commun.*, vol. 47, pp. 248–250, 1983.
[8] J.-M. Verdiell, M. A. Newkirk, T. L. Koch, R. P. Gnall, U. Koren, B. I. Miller, and L. L. Buhl, "Aspheric waveguide lenses for photonic integrated circuits," *Appl. Phys. Lett.*, vol. 62, pp. 808–810, 1993.
[9] J. H. Kim, "A collimation mirror in polymeric planar waveguide formed by reactive ion etching," *IEEE Photon. Technol. Lett.*, vol. 15, no. 3, pp. 422–424, Mar. 2003.
[10] C. Wei, F. Groen, M. K. Smit, I. Moerman, P. V. Daele, and R. Baets, "Integrated opical elliptic couplers: Modeling, design, and applications," *J. Lightw. Technol.*, vol. 15, no. 5, pp. 906–912, May 1997.
[11] K. Wörhoff, C. G. K. Roeloffzen, R. M. de Ridder, A. Driessen, and P. V. Lambeck, "Design and application of compact and highly tolerant polarization-independent waveguides," *J. Lightw. Technol.*, vol. 25, no. 5, pp. 1276–1283, May 2007.
[12] A. B. Vakhtin, D. J. Kane, W. R. Wood, and K. A. Peterson, "Common-path interferometer for frequency-domain optical coherence tomography," *Appl. Optics*, vol. 42, pp. 6953–6958, 2003.
[13] R. März, *Integrated Optics: Design and Modeling*. Norwood, MA: Artech House, 1995.
[14] J. M. Khosrofian and B. A. Garetz, "Measurement of a Gaussian laser beam diameter through the direct inversion of knife-edge data," *Appl. Optics*, vol. 22, pp. 3406–3409, 1983.
[15] J. Kalkman, A. V. Bykov, D. J. Faber, and T. G. van Leeuwen, "Multiple and dependent scattering effects in Doppler optical coherence tomography," *Opt. Exp.*, vol. 18, pp. 3883–3892, 2010.
[16] N. A. Nassif *et al.*, "In vivo high-resolution video-rate spectral-domain optical coherence tomography of the human retina and optic nerve," *Opt. Exp.*, vol. 12, pp. 367–376, 2004.
[17] T. G. van Leeuwen, D. J. Faber, and M. C. Aalders, "Measurement of the axial point spread function in scattering media using single-mode fiber-based optical coherence tomography," *IEEE J. Sel. Topic Quantum Electron.*, vol. 9, no. 2, pp. 227–233, Mar./Apr. 2003.
[18] S. Yuan and N. A. Riza, "General formula for coupling-loss characterization of single-mode fiber collimators by use of gradient-index rod lenses," *Appl. Opt.*, vol. 38, no. 15, pp. 3214–3222, 1999.
[19] H. Kogelnik and T. Li, "Laser beams and resonators," *Appl. Opt.*, vol. 5, pp. 1550–1567, 1966.
[20] I. Moerman, P. P. van Daele, and P. M. Demeester, "A review on fabrication technologies for the monolithic integration of tapers with III–V semiconductor devices," *IEEE Sel. Top. Quantum Electron.*, vol. 3, no. 6, pp. 1308–1320, Dec. 1997.

Van Duc Nguyen received the M.Sc. degree in physics from the University of Central Florida, in 2008. He is currently pursuing the Ph.D. degree at the Department of Biomedical Engineering and Physics, Academic Medical Center, University of Amsterdam, Amsterdam, The Netherlands.

His research focuses on using integrated optics in Optical Coherence Tomography (OCT) and on functional OCT.

Nur Ismail was born in Palermo, Italy, in 1977. He received the B.S. degree in electronic engineering at the University of Palermo, Italy, in 2002, the M.S. degree in information technology and telecommunications at CRES (Research Center for Electronics in Sicily), Monreale, Italy, in 2003, and the M.Sc. degree in photonics and optoelectronics from the University of Rome "Roma Tre", Italy, in 2006. He is currently pursuing the Ph.D. in the Integrated Optical MicroSystems (IOMS) group at the University of Twente, The Netherlands.

Between the years 2003 and 2006 he worked in the field of information technology in Rome, Italy.

Fei Sun received the M.S. degree in microelectronics from Xi'an Jiaotong University, China, in 2001, and the Ph.D. degree in optoelectronics from the Institute of Semiconductors, Chinese Academy of Sciences, Beijing, China, in 2006.

He worked as a Process Engineer in the Wuhan Research Institute for Posts and Telecommunications from 2001 to 2003, and as a post-doc in Wuhan National Laboratory for Optoelectronics from 2006 to 2008. Currently he is a Postdoctoral Researcher in Integrated Optical MicroSystems (IOMS) group, University of Twente, the Netherlands. His research interests are: design and fabrication of optical waveguide devices, Si-based integrated optics, and integration technology of photonic devices.

Kerstin Wörhoff received the M.Sc. degree in optoelectronics from the Technical University of Bratislava, Bratislava, Slovak Republic, in 1991 and the Ph.D. degree in applied physics from the University of Twente, Enschede, The Netherlands, in 1996.

In 1996, she joined the Lightwave Devices Group (now Integrated Optical MicroSystems Group, MESA + Institute for Nanotechnology), University of Twente, as a Postdoctoral Researcher. Since 2000, she has been an Assistant Professor with the same group. Her research interest covers the field of active and passive silicon-based photonics technology, rare-earth-ion doped devices, and integrated optical waveguide design.

Ton G. van Leeuwen studied physics at the University of Amsterdam and received the Ph.D. degree in 1993 from the Laboratory of Experimental Cardiology, University of Utrecht, The Netherlands.

Currently, he is head of the department of Biomedical Engineering and Physics, Academic Medical Center, University of Amsterdam, and Professor at the Biomedical Photonic Imaging group, University of Twente. His current research interests include the clinical application of biomedical optics.

Jeroen Kalkman received the M.Sc. degree in experimental physics in 1999 from the Vrije Universiteit Amsterdam, The Netherlands. He received the Ph.D. at the Institute for Atomic and Molecular Physics (AMOLF), Amsterdam where he worked on Erbium-doped photonic materials.

After working for two years at Philips NatLab in Eindhoven, The Netherlands, he moved to the Academic Medical Center in Amsterdam, The Netherlands. In this group he works on optical coherence tomography, light tissue interactions, and integrated optics for healthcare applications.